Thermal mass transport mechanism of an adatom on a crystalline surface

A. Roux [*] and N. Combe [†]

Centre d'Elaboration de Matériaux et d'Etudes Structurales, CNRS UPR 8011,
29 rue J. Marvig, BP 94347, F-31055 Toulouse cedex 4, France
and Université de Toulouse, UPS, F-31055 Toulouse, France

The diffusion of particles on surfaces subjected to a thermal gradient driven by phonons is numerically and theoretically investigated. Performing molecular dynamics (MD) simulations, we show that the thermal gradient induces a drift velocity of the adatom toward the cold regions. Beyond the bare study of the adatom trajectories for various thermal gradients, we propose to use a Massieu function as a thermodynamic potential that drives the adatom motion. We generalize the thermodynamic integration method to this out-of-equilibrium system to compute this thermodynamic potential. The thermal-gradient-induced effect is decorrelated from the stochastic diffusion from the analysis of the thermodynamic potential. Based on these results, we propose a model to evaluate the drift velocity and trajectory of an adatom that compares with a good agreement with trajectories provided by MD.

I. INTRODUCTION

Thermodiffusion (also known as thermophoresis or the Ludwig-Soret effect) is the motion of particles suspended in a liquid or gas in response to a thermal gradient. This phenomenon was first observed in liquids by Ludwig and Soret [1,2] and in gases by Tyndall and Strutt [3,4]. Onsager formalized the theoretical foundations of this phenomenon in the early 1930s [5]. In solids, this process is also known as thermomigration following Huntington suggestion [6], by analogy with electromigration.

Thermomigration has been experimentally used in solids since the early days of the transistor industry: noticeably, the fabrication of *pn* junctions used the thermal gradient zone melting method during which the doping of silicon by aluminum is achieved through the use of a thermal gradient [7–9]. Hence, because of its industrial applications, thermomigration has primarily been studied in bulk [10–13] while thermomigration on surfaces received less attention.

However, the shrinking of device dimensions in modern integrated circuits generates high resistance in the interconnects, resulting in concentrated Joule heating. This results in the formation of hotspots and nonuniform temperature distributions. In this scope, the coupling of electromigration and thermomigration has been experimentally characterized [14,15].

In addition, since the early 2000s, there has been a surge of interest in the development of new methods for transporting and controlling matter at the nanoscale especially for the synthesis of nanoparticles or nanodevices. Surface thermomigration is one of the mass transport mechanisms relevant to this aim. For instance, Schoen *et al.* [16,17] predicted that a gold nanoparticle confined in a carbon nanotube

subjected to a thermal gradient migrates to the cold regions, a prediction experimentally validated by transmission electron microscopy on similar systems [18,19]. Recently, the surface migration speed of vacancy islands on a Si(111) substrate has been measured by low energy electron microscopy at $0.18 \, \mathrm{nm \, s^{-1}}$ when applying a thermal gradient of $82 \, \mathrm{K \, cm^{-1}}$ [20]. In the growth community, surface thermomigration has been used to control the growth of a single-crystal aluminum nanowire [21].

Numerous theoretical and numerical simulations have investigated the thermal motion of concentric nanotubes [22–24] or of fullerene or small particles inside a nanotube [25–27]. Beyond this, exploiting the possibility to generate a displacement and thus a work from two heat baths, several authors have proposed some thermal nanomachine models and have numerically shown their operations [28–30]. The migration of a nano-object on a surface has also been highlighted in several theoretical and numerical studies [31–35].

Despite these investigations, the elementary mechanisms driving the thermomigration are far from being completely understood. In conductors, the heat flux primarily results from the displacement of free electrons, with only a minor contribution of phonons. Hence, thermomigration in these material is related to electromigration. Besides, in semiconductors and insulators, phonons are the main heat carriers. This paper focuses solely on these later materials where surface thermomigration of an object is driven by phonons traveling through the substrate. In his pioneer work, Huntington [6] compared several physical mechanisms presumably responsible of the thermomigration. He identifies (i) an intrinsic effective driving force [36,37] independent of the heat carriers and (ii) a force associated to the transfer of momentum from phonons [38]. While the transfer of momentum from phonons has been recently proposed to be responsible for the ballistic thermophoresis of clusters on a graphene sheet [33], following Huntington, the first mechanism, the intrinsic driving force is the dominant one in common solids: it corresponds to a

*auroux@cemes.fr
†nicolas.combe@cemes.fr

temperature effect regardless of the direction or nature (longitudinal or transversal) of the phonons interacting with the diffusing object.

In this latter case, quantitatively, following the standard treatments of irreversible thermodynamics, the mass flow in a thermal gradient reads

$$\vec{j} = -\frac{DcQ^*}{k_B T^2} \vec{\nabla} T, \qquad (1)$$

where Q^* is the atomic heat of transport, D the diffusion coefficient, c the atom concentration, and k_B the Boltzmann constant.

Several theories have related the coefficient Q^* to a migration energy [37]. In this paper, we propose to revise this problem and to study the elementary mechanisms of thermomigration of an adatom on a crystalline surface using molecular dynamic (MD) simulations. In particular, we will provide a formalism and a numerical approach to study thermomigration at the surface of crystalline solids: this method will enable us to explicitly determine the coefficient Q^*. We show that Q^* is not related to a migration energy but rather to a binding energy. After the description of the model in Sec. II, we evidence the thermomigration by analyzing adatom trajectories in Sec. III: the motion of the adatom is composed of a thermal-gradient-induced drift and a Brownian diffusive motion. In Sec. IV, we propose a quantitative numerical method based on the thermodynamic integration to measure a thermodynamic potential controlling the probability of presence of the adatom. From this potential, we decorrelate the thermal-gradient-induced response of the system from the Brownian diffusion process. Finally in Sec. V, we develop a kinetic model of the adatom thermomigration whose results are compared to trajectories derived from MD simulations.

II. SYSTEM AND METHODS

We simulate the thermomigration of an adatom on a crystalline surface subjected to a thermal gradient. Our analysis is restricted to the case where the heat flux is carried solely by phonons. As a result, MD simulations, a suitable tool for this modeling, are performed using the LAMMPS package [39].

A. Molecular dynamics

As a model case, we studied the diffusion of a single adatom on a (111) fcc surface submitted to a thermal gradient. Figure 1(a) reports a sketch of the simulation cell. The substrate is composed of a slab whose surface is perpendicular to the z direction. Periodic boundary conditions are applied in the x and y directions, respectively corresponding to the $[1\bar{1}0]$ and $[11\bar{2}]$ crystal structure directions. The substrate sizes along the x, y, and z directions are respectively $72.1a_0$, $13.78a_0$, and $16.7a_0$ with a_0 the lattice parameter. With these choices, the simulation box typically contains about 63 800 atoms. Sizes in the y and z directions are chosen to be high enough compared to the cutoff of the interatomic potential. In addition, with this choice, the effects due to the quantification of the phonon energies are limited. The size in the x direction results from a compromise between a sufficiently large size to observe the adatom diffusion and a small size to limit the
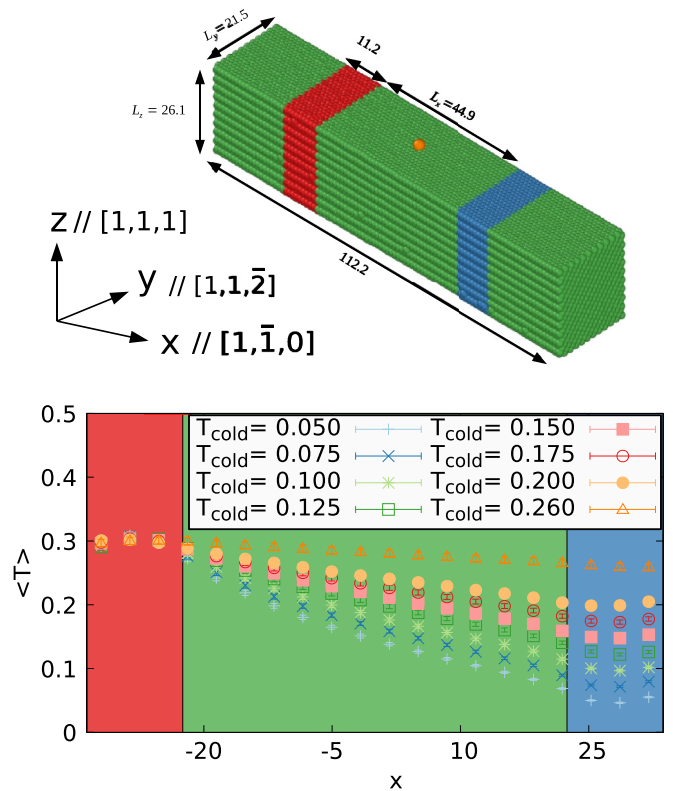

FIG. 1. (a) Sketch of the simulation model. Atoms of the hot and cold regions and the diffusing adatom are respectively in red, blue, and orange. (b) Temperature profiles (and standard deviations) in the substrate for $T_{\text{hot}} = 0.3$ and various values of T_{cold}. Standard deviations are so small that they are barely visible.

computational time. Because we want to understand the physical mechanisms underlying thermomigration independently of the precise details of the atomic potential, we have chosen to use a Lennard-Jones [40] (LJ) potential which minimizes the computational cost. The choice of a LJ potential is not singular for this problem since it has been used several times in the literature to model the interaction of nano-objects with graphene sheets subjected to a thermal gradient [32,33].

We fix the LJ potential parameters $\epsilon_{ss} = 1.0$, $\sigma_{ss} = 1.0$ between substrate atoms (mass $m_s = 1.0$), and $\epsilon_{as} = 0.82$, $\sigma_{as} = 1.0$ between the adatom (mass $m_a = 1.0$) and the substrate atoms. A $3.5\,\sigma_{ss}$ cutoff distance is applied. On the simulation timescale, these parameters warrant avoiding the observation of adatom evaporations or atomic exchange mechanisms. Below all quantities will be given in LJ units [41]: distances, masses, energies, times, and temperatures are expressed respectively in units of σ_{ss}, m_s, ϵ_{ss}, $\sqrt{\frac{m_s \sigma_{ss}}{\epsilon_{ss}}}$, and $\frac{\epsilon_{ss}}{k_B}$. Using LJ units, the lattice parameter a_0 is 1.56 (at 0 K) and $k_B = 1$.

B. Thermal gradient and temperature profile

The thermal gradient is applied by defining a hot and a cold slab region with thickness 11.2, normal to the x directions, and spaced by a distance 44.9 along the substrate. Two Nosé-Hoover thermostats (canonical *NVT* ensemble) are used to thermalize these regions at T_{hot} and T_{cold}. All other atoms of the cell (included the diffusing adatom) are in the

microcanonical (*NVE*) ensemble. Especially, the adatom under study and the substrate atoms with which it interacts are in the *NVE* ensemble. We have carefully checked that the use of Nosé-Hoover thermostats was satisfying by comparing our thermal gradient generation to other methods [42] and by comparing the thermal properties of the substrate with the literature [43]. The steady state of this system is reached once the Nosé-Hoover Hamiltonians of the hot and cold regions vary linearly with time, with opposite slopes proportional to the thermal flux in the substrate. We have checked that the velocity distributions of the adatom and interacting substrate atoms are accordingly Gaussian. We fix $T_{\mathrm{hot}} = 0.3$, below the fusion temperature $T_f \approx 0.69$ of the LJ potential [44]. T_{cold} varies from 0.05 to 0.26 to investigate various thermal gradients. Figure 1(b) shows the temperature profile along x in the substrate for various thermal gradients. Temperature profiles are measured from the average kinetic energy of 20 slabs of thickness 3.37 evenly distributed between the hot and cold regions. Both the time average temperature $\langle T \rangle$ and its standard deviation σ_T are measured and reported on Fig. 1(b); however standard deviations are so small that they are barely visible.

In Fig. 1(b), the temperature profiles between the hot and cold regions are linear in agreement with the standard Fourier law for small thermal gradient. Weak deviations from the linear behavior are observed for high thermal gradients: we have carefully checked that the steady state was not questioned in these cases. Such cases correspond to extremely strong thermal gradients: as an example, transposing the LJ parameters to a real material as copper [45] (for which $\epsilon = 0.4096\,\mathrm{eV}$, $\sigma = 0.2338\,\mathrm{nm}$, and $m = 105.49 \times 10^{-27}\,\mathrm{kg}$) would result in a thermal gradient of 113.37 K nm^{-1} for the smallest value of $T_{\mathrm{cold}} = 0.05$. In addition, the size of the simulation cell is comparable to the phonon mean free path so that part of the thermal transport is certainly ballistic in our simulations. Nevertheless, all these nonlinearities will have no effects on our analysis of Sec. IV and the kinetic model in Sec. V: we will exploit local thermal gradients and the size of the diffusing adatom is much smaller than the phonon mean free path and thus not sensitive to the ballistic or diffusive character of the thermal transport. Furthermore, discontinuities of temperatures are observed at the interfaces between the *NVE* and thermostatted regions: we attribute them to the existence of interface resistance or Kapitza resistance [46,47]. Due to the presence of these Kapitza resistances and the nonlinear temperature profile, there is a slight difference between the temperature variation per unit length $\frac{\Delta T}{L_x} = \frac{T_{\mathrm{hot}} - T_{\mathrm{cold}}}{L_x}$ and the average thermal gradient $\langle \frac{\partial T}{\partial x} \rangle = \frac{1}{L_x} \int_0^{L_x} \frac{\partial T}{\partial x} dx$ extracted from the temperature profile. Thus, below, the thermal gradient will be characterized by the average thermal gradient $\langle \frac{\partial T}{\partial x} \rangle$ whose values as a function of T_{cold} are given in Table I.

III. ADATOM TRAJECTORIES

The adatom is initially positioned without speed halfway between the hot and cold regions. Typical simulation times are about 5 million MD steps of 5×10^{-3} time units. For each investigated thermal gradient reported in Table I, we have performed 50 trajectories varying the y coordinate of the initial position of the adatom. Since we did not fix any substrate

TABLE I. Average thermal gradient $\langle \frac{\partial T}{\partial x} \rangle$ measured from the temperature profile as a function of T_{cold}.

T_{hot}	T_{cold}	$\langle \frac{\partial T}{\partial x} \rangle$
0.3	0.05	0.0038
0.3	0.075	0.0036
0.3	0.1	0.0033
0.3	0.125	0.0030
0.3	0.15	0.0027
0.3	0.175	0.0022
0.3	0.2	0.0017
0.3	0.225	0.0014
0.3	0.26	0.0008

atoms, the motion of two atoms can be investigated using the two surfaces of the substrate slabs enabling us to obtain two adatom trajectories from a single simulation. Figure 2 shows the adatom x coordinate as a function of time for five trajectories and for two thermal gradients $\langle \frac{\partial T}{\partial x} \rangle = 0.0038$ and 0.0027. These thermal gradients and trajectories are chosen as representative of our results. For all thermal gradients and calculated trajectories, the adatom jumps from a minima of the potential defined by the substrate to the neighboring one as shown in the inset of Fig. 2(a). The adatom motion is clearly diffusive and not in a ballistic regime; also no Lévy flight is observed.

For the highest thermal gradient 0.0038, regardless of the initial y coordinate, the adatom diffuses from its initial
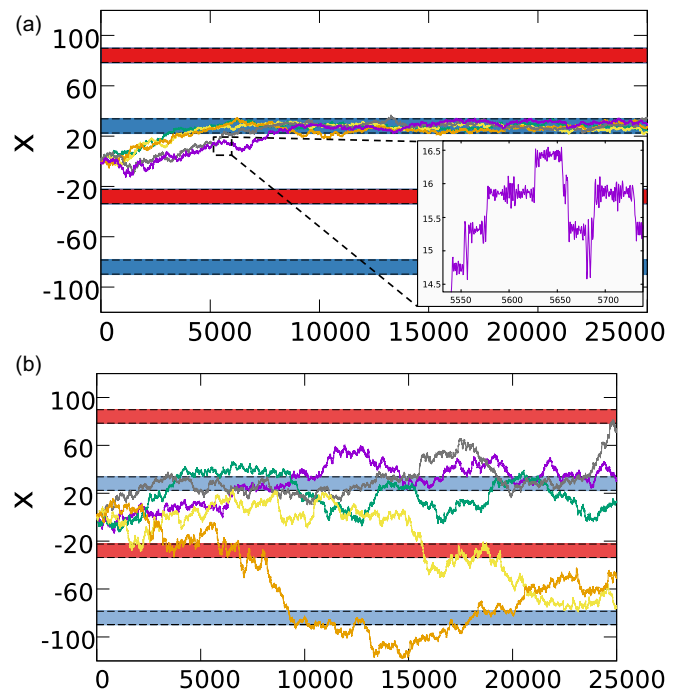

FIG. 2. The x coordinates of the adatom as a function of time (only 5 trajectories out of 50 calculated trajectories are represented); blue and red areas respectively designate cold and hot regions; (a) for $\langle \frac{\partial T}{\partial x} \rangle = 0.0038$ (the inset shows a zoom on a trajectory); (b) for $\langle \frac{\partial T}{\partial x} \rangle = 0.0027$.

position to the cold region evidencing a clear drift induced by the thermal gradient. Once it has entered the cold region, the adatom remains confined in it. We hence conclude that the cold area acts as an attractive well for the adatoms.

For the lowest thermal gradient 0.0027, the adatoms diffuse but the presence of a drift is less obvious than in the case of the highest thermal gradient. The adatoms may diffuse through the hot and/or cold regions. But most of the trajectories yield the adatoms in the vicinity of cold regions.

We conclude that the motion of the adatom is composed of a thermal-gradient-induced drift and a Brownian diffusive motion. To quantitatively separate these two contributions, we develop and use below a method based on the thermodynamic integration method [48] adapted to systems submitted to a thermal gradient.

IV. THERMODYNAMIC INTEGRATION

In this section, we propose a generalization of the standard thermodynamic integration (TI) method in order to calculate the thermodynamic potential controlling the x coordinates of the adatom in the presence of a thermal gradient. In standard TI [48], the free energy difference between two states is deduced from the integral over ensemble-averaged enthalpy changes along a thermodynamic path linking these states. Many versions of this algorithm including the use of out-of-equilibrium paths have been developed [49–51]. But to our knowledge, none of these methods applies for a system in a steady state submitted to a thermal gradient.

In a homogeneous temperature system at temperature T, the probability $p(x_0)$ to find the adatom at position x_0 would be controlled by its free energy $A(x_0)$ following $p(x_0) \propto \exp(-\frac{A(x_0)}{T})$.

In a system submitted to a thermal gradient, this concept can be extended provided that we make a local thermal equilibrium assumption. This assumption is justified in our case, since the characteristic time for the adatom diffusion (average time between two jumps in trajectories of Fig. 2) is longer than the characteristic time for its thermalization with the underlying substrate (of the order of the inverse of the oscillation frequency of the adatom in the crystalline potential well).

Under this local equilibrium assumption, we show in Appendix A that the probability $p(x_0)$ can be written as $p(x_0) \propto \exp[-\Phi(x_0)]$ with $\Phi(x_0)$ a thermodynamic potential. Because the temperature depends on the position, the appropriate thermodynamic potential controlling the position of the adatom is no longer the free energy $A(x_0)$ but a function reducing to $\frac{A}{T}$ in a system with a homogeneous temperature: indeed, in such a case, the function $\Phi = \frac{A}{T}$ is the opposite of the Massieu function $(S - \frac{U}{T})$ (Legendre transform of the entropy S, U designing the internal energy), and corresponds accordingly to a thermodynamic potential [52].

While the direct calculation of the thermodynamic potential $\Phi(x_0)$ is out of our computational capabilities because it would involve an integral over all microstates, it can be deduced from a TI scheme using the expression of its derivative

$\frac{\partial \Phi}{\partial x}$ (see Appendix A for derivation),

$$
\frac{\partial \Phi}{\partial x}(x_0) = \left\langle \frac{1}{T(x_0)} \frac{\partial V}{\partial x}(x_0, y, z) \right\rangle_{x_0} - \frac{1}{T^2(x_0)} \frac{\partial T}{\partial x}(x_0)
$$

$$
\times \left\langle \frac{\vec{p_a}^2}{2m_a} + \frac{1}{2} V(x_0, y, z) \right\rangle_{x_0}, \tag{2}
$$

where $x_0, y, z, \vec{p_a}$, and m_a are respectively the coordinates, momentum, and mass of the adatom and $V(x_0, y, z)$ is the interaction energy of the adatom with the substrate atoms. In Eq. (2), averages $\langle . \rangle_{x_0}$ are performed on the y, z coordinates and momentum $\vec{p_a}$ coordinates of the adatom at abscissa x_0 and over positions and momenta of substrate atoms. While the first right-hand term of Eq. (2) is standard in TI implementation (in homogeneous temperature systems), the second term is derived from the presence of the thermal gradient.

Technically, we calculate $\frac{\partial \Phi}{\partial x}(x_0)$ by TI: we perform MD simulations constraining the x coordinate of the adatom at position x_0 and we compute $\langle \frac{\partial V}{\partial x}(x_0, y, z) \rangle_{x_0}$, $\langle \frac{p_{a_y}^2 + p_{a_z}^2}{2m_a} \rangle_{x_0}$, and $\langle V(x_0, y, z) \rangle_{x_0}$. Since the constraint imposes the x-momentum component $p_{a_x} = 0$, we use the local thermal equilibrium assumption to rescale the kinetic energy following $\langle \frac{\vec{p_a}^2}{2m_a} \rangle_{x_0} = \frac{3}{2} \langle \frac{p_{a_y}^2 + p_{a_z}^2}{2m_a} \rangle_{x_0}$. The temperature $T(x_0)$ is evaluated from the temperature profile Fig. 1(b). Combining all these data yields the values of $\frac{\partial \Phi}{\partial x}$.

A. Thermodynamic potential

Figure 3(a) shows the derivative $\frac{\partial \Phi}{\partial x}(x_0)$ of the thermodynamic potential as a function of the adatom position x_0 for the thermal gradient $\langle \frac{\partial T}{\partial x} \rangle = 0.0038$. This function has a rising amplitude and a sinusoidal wave number ($k = 11.2$). We have checked that the wave number $k = \frac{2\pi}{a}$, where a is the projected distance in the x direction between two adatom stable sites on the surface, accordingly with the crystallography of the substrate surface.

Figure 3(b) shows the thermodynamic potential $\Phi(x_0)$ computed by numerical integration of $\frac{\partial \Phi}{\partial x}(x_0)$ for different thermal gradients. The thermodynamic potential $\Phi(x_0)$ is a combination of (i) a sinusoidal function and (ii) a slowly decreasing function, referred as the thermal-gradient-induced potential (TGIP) in the following. The sinusoidal function is yet another manifestation of the crystalline potential. The decreasing function, the TGIP, is related to the effect of the thermal gradient: it drives the adatom in the increasing x direction, i.e., toward the cold region. As observed on Fig. 3(b), the absolute slope of the TGIP increases with increasing thermal gradient.

In Fig. 3(b), the thermodynamic potential $\Phi(x_0)$ is plotted as a function of the x coordinate of the adatom. However, since the temperature profile also depends on the x coordinate of the adatom, the thermodynamic potential Φ could equivalently be plotted as a function of the inverse of the temperature $1/T$ (Fig. 4).[1]

---

[1]The natural variable for the Massieu function $S - \frac{U}{T}$ is the inverse of the temperature [52].
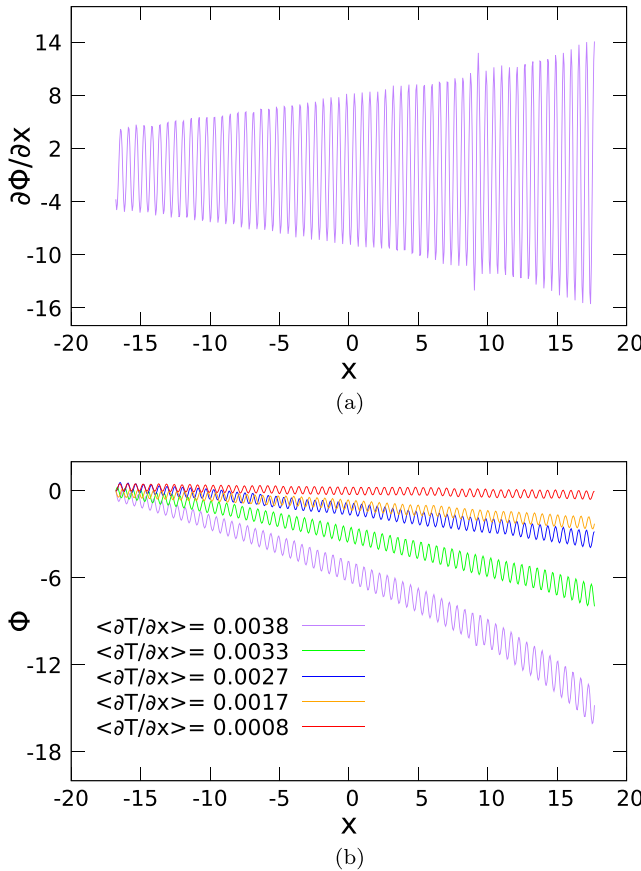
(a)

(b)

FIG. 3. (b) Thermodynamic potential and (a) its derivative as a function of the adatom position x_0 computed from simulations with the thermal gradient $\langle \frac{\partial T}{\partial x} \rangle = 0.0038$.

For all the investigated thermal gradients, the thermodynamic potential Φ as a function of $1/T$ appears to be a combination of a quasilinear $\Phi_{\text{TGIP}}(\frac{1}{T})$ and a sinusoidal $\Phi_{\text{diff}}(\frac{1}{T})$ function. $\Phi_{\text{TGIP}}(\frac{1}{T})$ is the curve that passes through all minima of the thermodynamic potential and $\Phi_{\text{diff}}(\frac{1}{T}) = \Phi(\frac{1}{T}) - \Phi_{\text{TGIP}}(\frac{1}{T})$. Interestingly, for all the investigated thermal gradients, the TGIP $\Phi_{\text{TGIP}}(\frac{1}{T})$ superimpose.
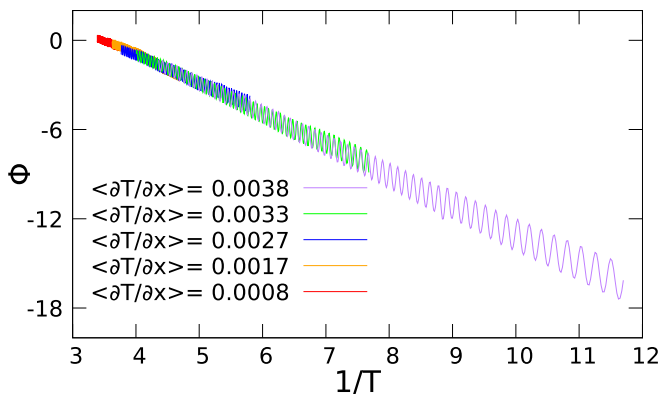

FIG. 4. Thermodynamic potential for several gradients as a function of the inverse of the temperature.

B. Interpretation of the thermodynamic potential

The quasilinear component $\Phi_{\text{TGIP}}(\frac{1}{T})$ of the thermodynamic potential $\Phi(\frac{1}{T})$ can be understood examining the behavior of the adatom at the minima of a crystalline potential well. Indeed, assuming a harmonic approximation and that the adatom is in local equilibrium with the substrate, we use the equipartition theorem to derive the average kinetic and potential energies of the adatoms: $\langle \frac{\vec{p_a}^2}{2m_a} \rangle_{x_0} = 3\frac{T(x_0)}{2}$ and $\langle V(x_0) \rangle_{x_0} = -V_0 + 3\frac{T(x_0)}{2}$ with V_0 the binding energy ($V_0 > 0$),[2] so that using Eq. (2),

$$\Phi(x_0)|_{\text{min}} \approx -\frac{V_0}{2T(x_0)} - \frac{9}{4}\ln[T(x_0)]. \quad (3)$$

Hence, we have detected all minima of the thermodynamic potential in Fig. 4 to compute $\Phi_{\text{TGIP}}(\frac{1}{T})$ and performed a regression using the following expression, $\Phi_{\text{TGIP}}(\frac{1}{T}) = -\frac{Q}{T} - C\ln(T) + \Phi_0$, with Φ_0 a physically meaningless constant. We extract $Q = 1.90 \pm 0.03$ and $C = -1.8 \pm 0.22$ for $\langle \frac{\partial T}{\partial x} \rangle = 0.0038$. Q and C respectively characterize the drift induced by the thermal gradient and the entropic effects. The relation between the coefficient Q and the heat of transport Q^* of Eq. (1) will be addressed in Sec. V. $Q = 1.90$ is in relatively good agreement with half the binding energy 4.17 of the adatom with the substrate calculated at 0 K. This conclusion has been reinforced by checking that the coefficient Q is proportional to the adatom-substrate interaction energy ϵ_{as}.[3] Besides, we found that the value of Q is independent of the values of the thermal gradients $\langle \frac{\partial T}{\partial x} \rangle = 0.0033$ and 0.0027 used to computed the thermodynamic potential.

$C = -1.8$ is in disagreement with the expected value $\frac{9}{4} = 2.25$ provided by the harmonic assumption above. Surprisingly it almost corresponds to the opposite to the expected value: we have checked carefully that this coincidence was not due to a sign error. For the gradients $\langle \frac{\partial T}{\partial x} \rangle = 0.0033$ and 0.0027, we extract $C = -1.57$ and -0.62 which evidences that the logarithmic corrections are not well resolved. To explain this disagreement, we argue that the harmonic assumption and the use of the equipartition theorem are questionable in this case since the adatom significantly diffuses along the y direction during the constrained MD simulations. Another presumably important effect is that our statistics are limited and the numerical integration used to calculated the thermodynamic potential Φ inevitably accumulates errors which prevents an accurate determination of C. In other word, we think that our calculations are not precise or reliable enough to be able to capture the logarithmic corrections.

To go forward with the examination of the thermodynamic potential $\Phi(\frac{1}{T})$, the diffusive behavior is characterized by the quantity $\Phi_{\text{diff}}(\frac{1}{T}) = \Phi(\frac{1}{T}) - \Phi_{\text{TGIP}}(\frac{1}{T})$ plotted in Fig. 5(a).

The function $\Phi_{\text{diff}}(\frac{1}{T})$ is an oscillating function whose amplitude A_{diff} increases as the temperatures decreases. Figure 5(b) shows the amplitude A_{diff} as a function of the inverse

---

[2]Since the motion of the adatom is constrained, it has only two degrees of freedom.
[3]The range of available values of $\epsilon_{as} \in [0.82 - 0.9]$ in MD simulations is limited to avoid the evaporation or exchange mechanisms on the simulation time scale.
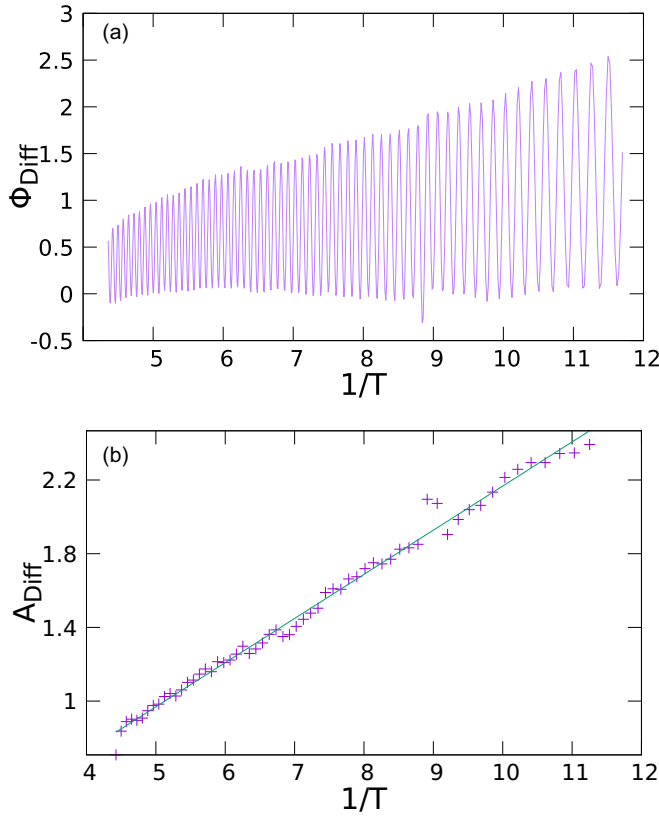
FIG. 5. (a) $\Phi_{\mathrm{diff}} = \Phi - \Phi_{\mathrm{TGIP}}$ as a function of the inverse of the temperature. (b) Amplitude A_{diff} of the oscillation of Φ_{diff} as a function of the inverse of the temperature and its affine regression (green solid line). Data are extracted from simulations with the thermal gradient $\langle \frac{\partial T}{\partial x} \rangle = 0.0038$.

of the temperature. The amplitude A_{diff} is related to the rate of diffusion of the adatom: this rate is expected to decrease as the temperature decreases since diffusion is slower at low temperature, an expectation in agreement with the results of Fig. 5(b).

Comparing the results of Fig. 5(b) with the values of A_{diff} computed for a substrate thermostatted with a homogeneous temperature, i.e., without a thermal gradient, we have checked that A_{diff} only depends on the temperature and not on its gradient.

The amplitude A_{diff} linearly increases with the inverse of the temperature with a slope $E_m = 0.239 \pm 0.003$. E_m is homogeneous to an energy and corresponds to the energy barrier for the diffusion of the adatom ($E_m > 0$). The measured value of E_m is slightly smaller than the energy barrier $E_b = 0.255$ for the adatom diffusion computed at 0 K.[4] Finally, we have checked that the amplitude A_{diff} (and thus E_m) is proportional to the adatom-substrate interaction energy ϵ_{as}.

---

[4]The energy barrier at 0K has been computed from potential energy minimizations constraining the x-position of the adatom. We have also checked that E_m agrees with the temperature dependence of the adatom diffusion coefficient on a thermostated substrate computed from the mean squared displacements of the adatom along trajectories.
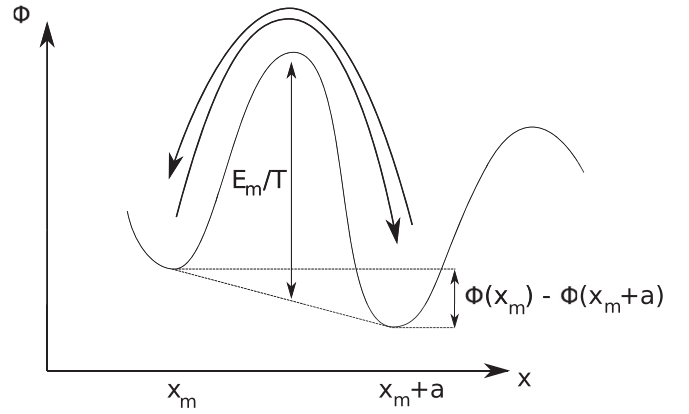

FIG. 6. Schematic representation of the thermodynamic potential as a function of the adatom position.

V. MODEL FOR THERMOMIGRATION

In this section, we propose a 1D kinetic model able to evaluate the average drift velocity induced by the thermal gradient.

A. Average drift velocity

Based on the results of Sec. IV, Fig. 6 schematically shows the thermodynamic potential seen by the adatom in the presence of a thermal gradient. Since this potential is asymmetric, the barriers to jump to the right or to the left are different. We estimate the probability rate of both jumps using a generalization of the transition-state theory (TST). Assuming the validity of the local thermodynamic equilibrium, the rate at which an adatom goes from a metastable state to a neighboring one can be derived generalizing the TST to a system showing a thermal gradient. The forward rate Eq. (B3) is calculated for a unidimensional system in Appendix B and is proportional to the quantity $e^{-[\Phi(x_m + \frac{a}{2}) - \Phi(x_m)]}$. x_m designs the abscissa of a metastable state of the thermodynamic potential and a is the projected distance in the x direction between two of these states. Therefore, the average velocity of the adatom reads

$$\langle v \rangle = a \left[\nu_+ e^{-[\Phi(x_m + \frac{a}{2}) - \Phi(x_m)]} - \nu_- e^{-[\Phi(x_m + \frac{a}{2}) - \Phi(x_m + a)]} \right], \quad (4)$$

with $\nu_{\pm}$ the attempt frequencies. For simplicity, we suppose that $\nu_+ = \nu_- = \nu_0$ in the following. Using the results of Sec. IV, $\Phi(x_m) = -\frac{Q}{T(x_m)}$ and $\Phi(x_m + a/2) = -\frac{Q}{T(x_m + a/2)} + \frac{E_m}{T(x_m + a/2)}$, the average velocity Eq. (4) deduces

$$\langle v \rangle = a^2 \nu_0 e^{-\Phi(x_m + \frac{a}{2})} Q e^{-\frac{Q}{T(x_m)}} \frac{d[1/T]}{dx}$$

$$= D[T] Q e^{\frac{(Q - E_m)a}{2} \frac{d[1/T]}{dx}} \frac{d[1/T]}{dx} \quad (5)$$

$$= -D[T] \frac{Q}{T^2} \left[e^{-\frac{(Q - E_m)a}{2T^2} \frac{dT}{dx}} \right] \frac{dT}{dx}, \quad (6)$$

with $D[T] = \nu_0 a^2 e^{(-\frac{E_m}{T})}$ the local diffusion coefficient of the adatom. As expected, Eq. (5) is compatible with a zero drift

velocity in the absence of a thermal gradient. As suggested in Eq. (1), the average velocity Eq. (6) does not only depend on the temperature gradient but also on the temperature itself.

Since Q is roughly half the binding energy of the adatom, Q is always a positive quantity. Hence, we find that the thermal gradient always drives the adatom toward the positive x, i.e., toward the cold region, so that a negative Soret coefficient is unreachable in this system.

The driving force pushing the adatom to the cold region is mainly an intrinsic effect: the decrease of the temperature increases its probability of presence $\propto \exp(Q/T)$. The entropic effects mentioned in Sec. IV A should induce some corrections to Eq. (5), but they are presumably weak and we have not been able to measure them. Finally, note that Eq. (5) originates from a first-order development of Eq. (4), but nothing prevents us from pushing this development to a higher order to address nonlinear effects.

Finally, from Eq. (5), one can identify the coefficient Q with the heat of transport Q^* in Eq. (1) providing that the thermal gradient is small enough to warrant that $e^{-\frac{(Q-E_m)a}{2T^2}\frac{dT}{dx}} \simeq 1$.

B. From the model to trajectories

In order to address the validity of Eq. (5), we calculate the model trajectory $x(t)$ of an adatom numerically solving the following differential equation:

$$\frac{dx}{dt} = -D[T]\frac{Q}{T^2}e^{-\frac{(Q-E_m)a}{2T^2}\frac{dT}{dx}}\frac{dT}{dx}. \tag{7}$$

Q is given in Sec. IV. The diffusion coefficient $D(T)$ as a function of temperature has been calculated from the mean squared displacement along trajectories of an adatom diffusing on a substrate thermostatted at an homogeneous temperature T.

Figures 7(a) and 7(b) show the model trajectories computed from Eq. (7) compared to the average MD trajectory $\langle x(t)\rangle_{\text{traj}}$ of the adatom at thermal gradients $\langle\frac{\partial T}{\partial x}\rangle = 0.0038$ and 0.0027. The average MD trajectory $\langle x(t)\rangle_{\text{traj}}$ of the adatom is computed by averaging the position $x(t)$ of the adatom at time t over all the trajectories computed by MD with the same initial conditions. We emphasize that there are no free parameters in the curves of Figs. 7(a) and 7(b).

So we presume that Murphy lacked vigilance since the agreement between the average MD trajectories of the adatom and the models of Eq. (7) is very good especially for time in the range [0–4000]. Note that we have intentionally limited the range of the abscissa of Figs. 7(a) and 7(b). Indeed when performing the average $\langle x(t)\rangle_{\text{traj}}$ at time t over all the trajectories, we elude the trajectories which have joined the cold region at a time $t' < t$. So when time t increases, the number of trajectories involved in the average not only decreases, but the estimation of $\langle x(t)\rangle_{\text{traj}}$ is biased by the fact that the average is computed on trajectories that have not reached the cold region yet.

VI. DISCUSSION

We think that the good agreement between the prediction of our model and MD simulations results shown in Fig. 7
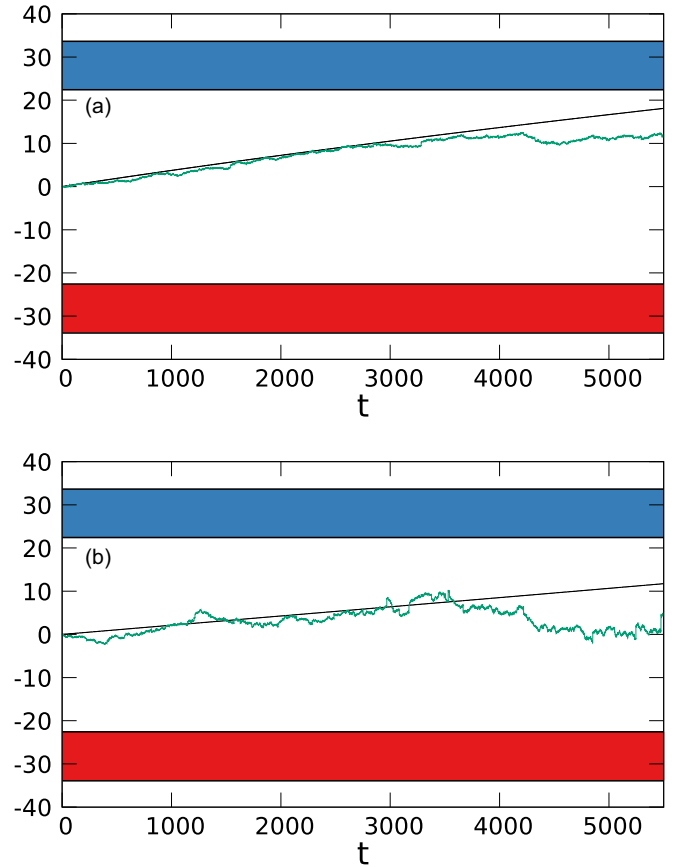

FIG. 7. Model trajectory (solid black line) computed from integration of Eq. (7) compared to the average MD trajectory of the adatom; (a) for $\langle\frac{\partial T}{\partial x}\rangle = 0.0038$; (b) for $\langle\frac{\partial T}{\partial x}\rangle = 0.0027$.

gives an additional justification of our different assumptions to derive the model Eq. (6): noticeably, the adatom diffuses on the surface and is locally in thermal equilibrium with the substrate. Hence, the heat of transport Q^* depends on the binding energy of the adatom with the substrate and weakly depends on the migration energy E_m. This result is in opposition with previous theories [36]. We emphasize that in our simulations, we found $Q = 1.9$ while $E_m = 0.23$ so that both quantities differ by a factor of 8, almost an order of magnitude: a model involving a heat of transport Q^* equal to the migration energy as proposed previously would definitely not produce a good agreement with MD simulations results. We think that the main difference between our model and previous ones is that we introduce the thermodynamic potential (a Massieu function) Φ which drives the adatom probability of presence in an inhomogeneous temperature system.

Moreover, concerning Eq. (5), in our MD simulations, we evaluate the coefficient $e^{-\frac{(Q-E_m)a}{2T^2}\frac{dT}{dx}} \simeq 0.84$ with $Q = 1.9$, $E_m = 0.23$, $T = 0.1$, and $\frac{dT}{dx} = 0.0038$. Hence, nonlinear effects, i.e., the adatom average velocity reads as a series of powers of $\frac{dT}{dx}$, are significant and could not be eluded in our simulations. However, in realistic experimental conditions where the thermal gradient is several orders of magnitude smaller that in our simulations, the coefficient $e^{-\frac{(Q-E_m)a}{2T^2}\frac{dT}{dx}}$ should be one to a very good approximation. Equation (5) then

agrees with Eq. (1) with Q^* equal to half the binding energy of the adatom.

VII. CONCLUSION

In this paper, we have numerically and theoretically studied the diffusion of an adatom on a surface submitted to a thermal gradient. The thermal gradient drives the adatom toward the cold regions. We have shown that (i) the Massieu function is the suitable thermodynamic potential to investigate this out-of-equilibrium steady-state system. (ii) We have provided a method generalizing the thermodynamic integration method to compute it. Analyzing this thermodynamic potential, we have been able to decorrelate the thermal-gradient-induced effect from the stochastic diffusion. (iii) We have shown that the atomic heat transport characterizing the thermal-gradient-induced effect is proportional to the binding energy of the adatom with the substrate. Based on these results and (iv) generalizing the transition-state theory to systems submitted to thermal gradient, (v) we have proposed a model to evaluate the drift velocity of an adatom and to evidence the main physical processes operating during the thermomigration process. Our model agrees very well with MD simulation results. It also agrees with the standard treatment of mass transport Eq. (1) by irreversible thermodynamics.

The main driving force for the thermomigration is the so-called intrinsic effect, i.e., the increase of the probability of presence $\propto \exp(Q/T)$ of the adatom with the decrease of temperature, where Q is found to be mainly independent of the temperature. Our results show that the thermomigration always drives an adatom diffusing on a surface toward the cold region and that a negative Soret coefficient is unreachable.

We cite below two perspectives to this work. First, all of our results are based on a local thermodynamic equilibrium assumption. However, this local thermodynamic equilibrium assumption has some limitations both for the evaluation of the TST rate and the probability distribution [53,54]: investigating the corrections to the local thermodynamic equilibrium assumptions would certainly allow a better understanding of the thermomigration phenomenon. Especially, our approach would certainly be arguable if the diffusion of the adatom was faster enough to prevent its local thermalization with the substrate.

Second, the thermomigration of a cluster involves some elastic effects that would be worth investigating especially for comparison with experiments. In addition, elastic effects could potentially enable a negative Soret coefficient.

APPENDIX A: THERMODYNAMIC INTEGRATION FOR A SYSTEM SUBMITTED TO A THERMAL GRADIENT

Let $\vec{r}_a$, $\vec{p}_a$ and $\vec{r}_i$, $\vec{p}_i$ be the positions and momentum of the adatom and of the substrate atoms with $i \in \{1, N\}$. The Hamiltonian of the investigated system reads

$$H(\vec{r}_a, \vec{p}_a, \vec{r}_i, \vec{p}_i) = \frac{p_a^2}{2m_a} + \sum_i \frac{p_i^2}{2m_i} + \sum_i E_{LJ}(\vec{r}_a, \vec{r}_i) + \frac{1}{2}\sum_{i \neq j} E_{LJ}(\vec{r}_i, \vec{r}_j). \tag{A1}$$

In the presence of a thermal gradient and under the local thermal equilibrium assumption, the probability to observe the adatom at a position with abscissa x_0 is [53,54]

$$p(x_0) = \frac{Z(x_0)}{Z}, \tag{A2}$$

$$Z(x_0) = \frac{1}{h^{3N+3}} \int \delta(x_a - x_0) e^{[-\int \beta(\vec{r})\mathcal{H}(\vec{r})d^3\vec{r}]} d^3\vec{r}_a d^3\vec{p}_a \prod_{i=1}^{N} d^3\vec{r}_i d^3\vec{p}_i, \tag{A3}$$

$$Z = \frac{1}{h^{3N+3}} \int e^{[-\int \beta(\vec{r})\mathcal{H}(\vec{r})d^3\vec{r}]} d^3\vec{r}_a d^3\vec{p}_a \prod_{i=1}^{N} d^3\vec{r}_i d^3\vec{p}_i, \tag{A4}$$

where $\beta(\vec{r}) = \frac{1}{T(\vec{r})}$ states for the temperature dependence and $\mathcal{H}(\vec{r})$ is the microscopic many-body Hamiltonian density,

$$\mathcal{H}(\vec{r}) = \delta(\vec{r}_a - \vec{r})\left[\frac{p_a^2}{2m_a} + \frac{1}{2}\sum_i E_{LJ}(\vec{r}_a, \vec{r}_i)\right] + \sum_i \delta(\vec{r}_i - \vec{r})\left[\frac{p_i^2}{2m_i} + \frac{1}{2}E_{LJ}(\vec{r}_a, \vec{r}_i) + \sum_{j \neq i}\frac{1}{2}E_{LJ}(\vec{r}_i, \vec{r}_j)\right]. \tag{A5}$$

In the present study, $T(\vec{r})$ only depends on x: $T(\vec{r}) = T(x)$. From Eq. (A5), we hence deduce

$$\int \beta(\vec{r})\mathcal{H}(\vec{r}) = \frac{p_a^2}{2m_a T(x_a)} + \frac{1}{2}\sum_i E_{LJ}(\vec{r}_a, \vec{r}_i)\left[\frac{1}{T(x_a)} + \frac{1}{T(x_i)}\right] + \sum_i \frac{p_i^2}{2m_i T(x_i)} + \frac{1}{2}\sum_i\sum_{j\neq i}\frac{E_{LJ}(\vec{r}_i, \vec{r}_j)}{T(x_i)}. \quad \text{(A6)}$$

Defining $\Phi(x_0) = -\ln[Z(x_0)]$, the derivative of $\Phi(x_0)$ compared to x_0 is deduced from Eqs. (A2) and (A6):

$$\frac{\partial \Phi}{\partial x}(x_0) = -\frac{\frac{\partial Z}{\partial x}}{Z}(x_0) = -\left\langle\left[\frac{\vec{p}_a^2}{2m_a} + \sum_i \frac{1}{2}E_{LJ}(\vec{r}_a^0, \vec{r}_i)\right]\frac{1}{T(x_0)^2}\frac{\partial T}{\partial x}(x_0)\right\rangle_{x_0} + \left\langle\sum_i \frac{1}{2}\frac{\partial E_{LJ}}{\partial x_a}(\vec{r}_a^0, \vec{r}_i)\left[\frac{1}{T(x_0)} + \frac{1}{T(x_i)}\right]\right\rangle_{x_0}, \quad \text{(A7)}$$

with $\vec{r}_a^0 = (x_0, y_a, z_a)$. $\langle.\rangle_{x_0}$ designs an average over all space variables y_a, z_a, $\vec{p}_a$, $\vec{r}_i$, and $\vec{p}_i$ with $i \in \{1, N\}$ while the abscissa x_a of the adatom equals $x_a = x_0$.

Finally, since the relative temperature variation over the LJ cutoff length scale λ, $\frac{1}{T}\frac{\partial T}{\partial x} \ll \frac{1}{\lambda}$, is weak, we approximate $\frac{1}{T(x_i)} \simeq \frac{1}{T(x_0)}$ when the substrate atom at abscissa x_i interacts with the adatom at abscissa x_0:

$$\frac{\partial \Phi}{\partial x} = -\left\langle\left[\frac{\vec{p}_a^2}{2m_a} + \sum_i \frac{1}{2}E_{LJ}(\vec{r}_a^0, \vec{r}_i)\right]\frac{1}{T(x_0)^2}\frac{\partial T}{\partial x}(x_0)\right\rangle_{x_0} + \left\langle\frac{1}{T(x_0)}\sum_i\frac{\partial E_{LJ}(\vec{r}_a^0, \vec{r}_i)}{\partial x_a}\right\rangle_{x_0} \quad \text{(A8)}$$

$$= -\left\langle\left[\frac{\vec{p}_a^2}{2m_a} + \frac{1}{2}V(\vec{r}_a^0)\right]\frac{1}{T(x_0)^2}\frac{\partial T}{\partial x}(x_0)\right\rangle_{x_0} + \left\langle\frac{1}{T(x_0)}\frac{\partial V}{\partial x_a}(\vec{r}_a^0)\right\rangle_{x_0}, \quad \text{(A9)}$$

where $V(\vec{r}_a^0) = \sum_i E_{LJ}(\vec{r}_a^0, \vec{r}_i)$.

APPENDIX B: TRANSITION-STATE THEORY WITH A THERMAL GRADIENT

In this section, using the transition-state theory (TST), we calculate the forward rate k_{TST}^+, i.e., the probability per unit time that a system submitted to a thermal gradient goes from a metastable state to a neighboring one crossing a transition state. For simplicity, we derive here the forward rate k_{TST}^+ for a unidimensional system. The generalization to a multidimensional potential is not simple except perhaps if the thermal gradient is perpendicular to the transition-state hyperplane, but even this simpler case is out of the scope of this study. So we suppose a unidimensional particle of mass m, position x, and momentum $p = m\dot{x}$. This particle interacts with a wider system with many degrees of freedom (the substrate in the present case), so that the dynamic of the particle can be derived from a reduction procedure yielding to an effective potential $V(x)$ driving the particle motion [55]. We suppose that this effective potential $V(x)$ shows two metastable states x_1 and $x_2 > x_1$ divided by a transition state at x_t. See Fig. 8.
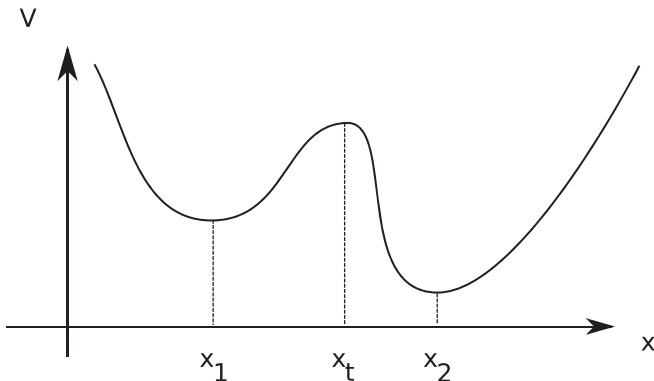

FIG. 8. Sketch of the effective potential seen by the particle.

We limit our development to the simple case where all timescales of the system (substrate + particle) are separable, and we assume that (i) the local thermodynamic equilibrium prevails for all degree of freedom (including the degree of freedom of the particle and the ones of the substrate) and that (ii) any trajectory of the particle that crosses the transition x_t will not recross it [55]. The assumption (ii) is standard for TST and assumption (i) is a generalization of the standard thermodynamic equilibrium assumption for TST. Within these assumptions, the forward rate, i.e., the probability per unit time that the particle goes from the metastable state in x_1 to the one in x_2, reads [55]

$$k_{\text{TST}}^+ = \frac{\int dx\,dp\,\delta(x - x_t)\frac{p}{m}\theta(p)e^{-\beta(x)(\frac{p^2}{2m} + V(x))}}{\int_{\text{initial well}} dx\,dp\,e^{-\beta(x)(\frac{p^2}{2m} + V(x))}},$$

with $\theta(x) = 1$ for $x > 0$ and 0 otherwise,

$$k_{\text{TST}}^+ = \frac{e^{-\beta(x_t)V(x_t)}\int_0^{+\infty} dp\,\frac{p}{m}e^{-\beta(x_t)\frac{p^2}{2m}}}{\int_{\text{initial well}} dx\,dp\,e^{-\beta(x)(\frac{p^2}{2m} + V(x))}},$$

with

$$\int_0^{+\infty} dp\,\frac{p}{m}e^{-\beta(x_t)\frac{p^2}{2m}} = \frac{1}{\beta(x_t)}$$

and

$$\int_{\text{initial well}} dx\,dp\,e^{-\beta(x)\left(\frac{p^2}{2m} + V(x)\right)}$$
$$= \int_{x<x_t} dx\left[e^{-\beta(x)V(x)}\int_{-\infty}^{\infty} dp\,e^{-\beta(x)\frac{p^2}{2m}}\right]$$
$$= \int_{x<x_t} dx\left[e^{-\beta(x)V(x)}\sqrt{\frac{2\pi m}{\beta(x)}}\right].$$

The function $e^{-\beta(x)V(x)}$ is only significant in the vicinity of the minima $x_{\min}$ of the function $\beta(x)V(x)$. Hence, we can approximate $\beta(x)V(x) = \beta(x_{\min})V(x_{\min}) + \frac{(x-x_{\min})^2}{2}\frac{d^2(\beta V)}{dx^2}(x_{\min})$ to get

$$\int_{\text{initial well}} dx\,dp\, e^{-\beta(x)(\frac{p^2}{2m}+V(x))}$$

$$\simeq \sqrt{\frac{2\pi m}{\beta(x_{\min})}}\, e^{-\beta(x_{\min})V(x_{\min})}\sqrt{\frac{2\pi}{\frac{d^2(\beta V)}{dx^2}(x_{\min})}}.$$

So finally, we get

$$k_{\text{TST}}^+ = \frac{e^{-\beta(x_t)V(x_t)}}{e^{-\beta(x_{\min})V(x_{\min})}}\frac{1}{2\pi\beta(x_t)}\sqrt{\frac{\beta(x_{\min})\frac{d^2(\beta V)}{dx^2}(x_{\min})}{m}}. \quad (B1)$$

In the case of the thermomigration of an adatom on a crystalline substrate, the length scale of the temperature variation is very weak compared to the one of the variation of the potential $V(x)$; the minima x_1 of the potential $V(x)$ almost coincides with the minima of the function $\beta(x)V(x)$: $x_{\min} \approx x_1$, so that

within a good approximation, k_{TST}^+ reads

$$k_{\text{TST}}^+ = \frac{e^{-\beta(x_t)V(x_t)}}{e^{-\beta(x_1)V(x_1)}}\frac{1}{2\pi\beta(x_t)}\sqrt{\frac{\beta(x_1)\frac{d^2(\beta V)}{dx^2}(x_1)}{m}} \quad (B2)$$

$$= \nu_+ e^{-[\beta(x_t)V(x_t)-\beta(x_1)V(x_1)]}, \quad (B3)$$

with $\nu_+ = \frac{1}{2\pi\beta(x_t)}\sqrt{\frac{\beta(x_1)\frac{d^2(\beta V)}{dx^2}(x_1)}{m}}$. Equation (B2) is equivalent to the result of the TST theory when the temperature is independent of the position [55].

Including the entropic terms of the prefactor in the exponential, Eq. (B2) would involve the thermodynamic potential ϕ so that $k_{\text{TST}}^+ \propto e^{-[\phi(x_t)-\phi(x_1)]}$.

We note that Eq. (B3) differs from previous theories [36] where the rate at which an adatom goes from a metastable state to a neighboring one only depends on the adatom temperature in its initial metastable state (and not on the one at the barrier). Nevertheless, we argue that these former expressions [36] do not satisfy the detailed balance whereas Eq. (B3) does.

[1] C. Ludwig, Sitz.-ber. Akad. Wiss. Wien, Math. Nat. Kl **20**, 539 (1856).

[2] Ch. Soret, J. Phys. Theor. Appl. **9**, 331 (1880).

[3] J. Tyndall, Nature (London) **1**, 339 (1870).

[4] R. J. Strutt, Proc. R. Soc. London **34**, 414 (1883).

[5] L. Onsager, Phys. Rev. **37**, 405 (1931).

[6] H. Huntington, J. Phys. Chem. Solids **29**, 1641 (1968).

[7] W. Pfann, JOM **7**, 961 (1955).

[8] E. Y. Buchin and Y. I. Denisenko, Proc. SPIE **6260**, 62601L1 (2006).

[9] M. Eslamian and Z. Saghir, Fluid Dyn. Mater. Process. **8**, 353 (2012).

[10] J. Janek and H. Timm, J. Nucl. Mater. **255**, 116 (1998).

[11] D. Peterson and S. J. Kim, J. Less-Common Met. **141**, 249 (1988).

[12] M. Uz and O. Carlson, J. Less-Common Met. **116**, 317 (1986).

[13] B. Ernst, G. Frohberg, K. Kraatz, and H. Wever, in *Diffusion in Materials DIMAT 1996*, Defect and Diffusion Forum Vol. 143 (Trans Tech Publications, 1997), pp. 1649–1654.

[14] N. Somaiah and P. Kumar, J. Appl. Phys. **124**, 185102 (2018).

[15] Y. Kimura and Y. Ju, AIP Adv. **10**, 085125 (2020).

[16] P. A. E. Schoen, J. H. Walther, S. Arcidiacono, D. Poulikakos, and P. Koumoutsakos, Nano Lett. **6**, 1910 (2006).

[17] P. A. E. Schoen, J. H. Walther, D. Poulikakos, and P. Koumoutsakos, Appl. Phys. Lett. **90**, 253116 (2007).

[18] A. Barreiro, R. Rurali, E. R. Hernández, J. Moser, T. Pichler, L. Forró, and A. Bachtold, Science **320**, 775 (2008).

[19] H. Somada, K. Hirahara, S. Akita, and Y. Nakayama, Nano Lett. **9**, 62 (2009).

[20] F. Leroy, A. E. Barraj, F. Cheynis, P. Müller, and S. Curiotto, Phys. Rev. Lett. (to be published).

[21] D. Xie, Z.-Y. Nie, S. Shinzato, Y.-Q. Yang, F.-X. Liu, S. Ogata, J. Li, E. Ma, and Z.-W. Shan, Nat. Commun. **10**, 4478 (2019).

[22] Q.-W. Hou, B.-Y. Cao, and Z.-Y. Guo, Nanotechnology **20**, 495503 (2009).

[23] V. R. Coluci, V. S. Timóteo, and D. S. Galvão, Appl. Phys. Lett. **95**, 253103 (2009).

[24] J. Leng, Z. Guo, H. Zhang, T. Chang, X. Guo, and H. Gao, Nano Lett. **16**, 6396 (2016).

[25] R. Rurali and E. Hernández, Chem. Phys. Lett. **497**, 62 (2010).

[26] W. Yao and C. Basaran, Int. J. Damage Mech. **23**, 203 (2013).

[27] A. V. Savin and O. I. Savina, Phys. Solid State **63**, 811 (2021).

[28] Z.-Y. Guo, Q.-W. Hou, and B.-Y. Cao, J. Heat Transfer **134**, 051010 (2012).

[29] F. Zhu, Z. Guo, and T. Chang, Appl. Mater. Today **18**, 100520 (2020).

[30] R. L. Zhang, S. Y. Li, Y. Li, and M. F. Wang, J. Nano Res. **74**, 97 (2022).

[31] A. Savin and Y. Kivshar, Sci. Rep. **2**, 1012 (2012).

[32] M. Becton and X. Wang, J. Chem. Theory Comput. **10**, 722 (2014).

[33] E. Panizon, R. Guerra, and E. Tosatti, Proc. Natl. Acad. Sci. USA **114**, 201708098 (2017).

[34] R. Rajegowda, S. K. Kannam, R. Hartkamp, and S. P. Sathian, Nanotechnology **29**, 215401 (2018).

[35] A. V. Savin, Phys. Rev. B **106**, 205410 (2022).

[36] J. A. Brinkman, Phys. Rev. **93**, 345 (1954).

[37] G. Schottky, Phys. Status Solidi B **8**, 357 (1965).

[38] V. B. Ficks, Sov. Phys. Solid State **3**, 724 (1961).

[39] A. P. Thompson, H. M. Aktulga, R. Berger, D. S. Bolintineanu, W. M. Brown, P. S. Crozier, P. J. in 't Veld, A. Kohlmeyer, S. G. Moore, T. D. Nguyen, R. Shan, M. J. Stevens, J. Tranchida, C. Trott, and S. J. Plimpton, Comput. Phys. Commun. **271**, 108171 (2022).

[40] J. E. Lennard-Jones, Proc. Phys. Soc. **43**, 461 (1931).

[41] M. Allen and D. Tildesley, *Computer Simulation of Liquids* (Clarendon Press, 1987).

[42] P. Wirnsberger, D. Frenkel, and C. Dellago, J. Chem. Phys. **143**, 124104 (2015).

[43] P. Chantrenne and J. Barrat, J. Heat Transfer **126**, 577 (2004).

[44] E. A. Mastny and J. J. de Pablo, J. Chem. Phys. **127**, 104504 (2007).

[45] P. Guan, D. R. Mckenzie, and B. A. Pailthorpe, J. Phys.: Condens. Matter **8**, 8753 (1996).

[46] P. Kapitza, in *Helium 4*, edited by Z. Galasiewicz (Pergamon, 1971), pp. 114–153.

[47] E. T. Swartz and R. O. Pohl, Rev. Mod. Phys. **61**, 605 (1989).

[48] D. Frenkel and B. Smit, *Understanding Molecular Simulation*, 2nd ed. (Academic Press, 2002).

[49] J. G. Kirkwood, J. Chem. Phys. **3**, 300 (1935).

[50] D. Frenkel and A. J. C. Ladd, J. Chem. Phys. **81**, 3188 (1984).

[51] R. Freitas, M. Asta, and M. de Koning, Comput. Mater. Sci. **112**, 333 (2016).

[52] H. B. Callen, *Thermodynamics and an Introduction to Thermo-statistics*, 2nd ed. (John Wiley and Sons, 1985).

[53] H. Mori, Phys. Rev. **112**, 1829 (1958).

[54] P. Anzini, G. M. Colombo, Z. Filiberti, and A. Parola, Phys. Rev. Lett. **123**, 028002 (2019).

[55] P. Hänggi, P. Talkner, and M. Borkovec, Rev. Mod. Phys. **62**, 251 (1990).